Mechanoenzymes under superstall and large assisting loads reveal structural features

Denis Tsygankov and Michael E. Fisher*

Institute for Physical Science and Technology, University of Maryland, College Park, MD 20742

Contributed by Michael E. Fisher, October 19, 2007 (sent for review September 5, 2007)

Single-molecule experiments on the motor protein kinesin have observed runs of backsteps and thus a negative, that is, *reverse* mean velocity, *V*, under superstall loads, *F*; but, counterintuitively, beyond stall, *V*(*F*) displays a shallow *minimum* and then *decreases* in magnitude. Conversely, under *assisting* loads *V*(*F*) rises to a *maximum* before decreasing monotonically. By contrast, while the velocity of myosin V also saturates under assisting loads, the motor moves backward increasingly rapidly under superstall loads. For both kinesin and myosin V this behavior is implied remarkably well by simple two-state kinetic models when extrapolated to large loads. To understand the origins of such results in general mechanoenzymes, biochemical kinetic descriptions are discussed on the basis of a free-energy landscape picture. It transpires that the large-load performance is determined by the geometrical placement of the intermediate mechanochemical states of the enzymatic cycles relative to the associated transition states. Explicit criteria are presented for *N*-state sequential kinetics, including side-reaction chains, etc., and for parallel-pathway models. Physical colocalization of biochemically distinct states generally implies large-load velocity saturation.

backsteps | biomechanochemical kinetics | free-energy landscape | motor proteins | velocity saturation

Single-molecule studies of motor proteins and other mechanoenzymes (1–4) under varying imposed loads aim to uncover features of the underlying biochemical structure and mechanisms. Thus, in recent experiments (5, 6) on conventional kinesin, a highly processive motor, the mean velocity, V, along the microtubule track (which we will suppose is aligned with the positive x axis) has been measured, at various concentrations of ATP, as a function of an imposed load $\mathbf{F} = (F_x, F_y, F_z)$ in both *resisting* and *assisting* regimes. [Sideways and oblique loads have also been examined (5, 7).]

Observed Behavior and Large-Load Extrapolations

Fig. 1 displays the data of Block and coworkers (5) as the x component of $\mathbf{F}$ varies (with $F_y = 0$). In the resisting regime, $F_x < 0$, shown on the right, the observations extend up to a stall force of $F_S \simeq -(6–7)$ pN at which, by definition, the velocity vanishes. The assisting regime, $F_x > 0$, extends on the left to $F_x \simeq +8$ pN. Remarkably, "helping the motor" by pulling it in the positive (or "designed") direction, results in a *decreasing* velocity at high [ATP]. At low [ATP] the assistance does at first increase the speed; but then V appears to reach a relatively low maximum. This unexpected behavior is well captured by the solid curves, which represent a theoretical fit (8, 9) that recognizes the *vectorial* character of the load $\mathbf{F}$ transmitted to the motor body. The fit at low [ATP] suggests that $V(F_x)$ would *also* decrease quite rapidly at larger loads.

Perhaps more surprising is the behavior predicted by the extensions of the fitted plots into the *superstall regime* where the resistive load $|F_x|$ exceeds $|F_S|$. Then, the velocity changes sign and becomes negative, corresponding to a reverse or backstepping motion. However, the speed remains small, 10–30 nm/s; furthermore, some 20–30% beyond F_S the plots undergo shallow *minima*, and thereafter, $V(F_x)$ approaches zero from below.

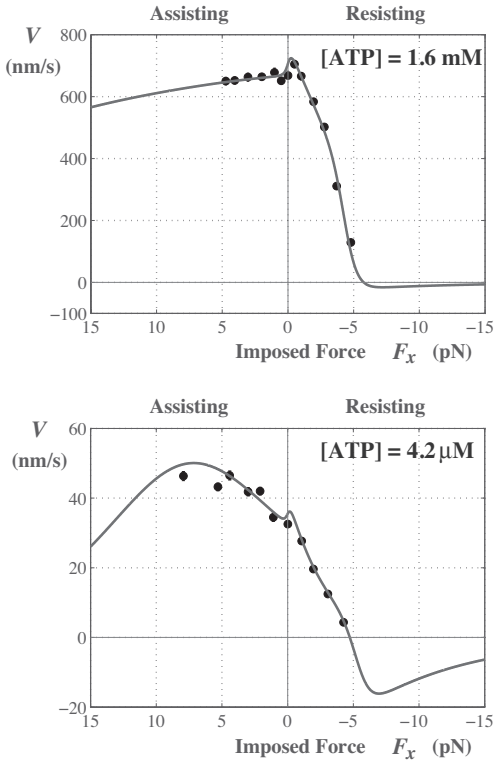

Fig. 1. Velocity vs. x component of the load $\mathbf{F}$ for kinesin. The data, for [ATP] = 1.6 nm and 4.2 μM are from Block *et al.* (5) and the fits to a two-state kinetic model embodying a free-energy landscape picture are from Fisher and Kim (8).

These predictions were not reported originally (8) and, indeed, might well be regarded as merely representing an unwarranted extrapolation of theory into a totally new domain of motor operation (10). Nevertheless, as seen in Fig. 2, when Carter and Cross (6) explored this highly resisting superstall regime just such low, 10–40 nm/s, backward velocities emerged. Furthermore, unambiguous minima appeared, albeit at somewhat higher loads. What might be the implications of this seemingly anomalous behavior?

The Carter–Cross data in Fig. 2 for assisting ($F_x > 0$) loads also confirm the conclusions from Block *et al.* (5) regarding the decrease of V at high [ATP]: despite the noise, a clear drop-off is seen for $F_x \gtrsim 5$ pN. Similarly, at [ATP] = 10 μM, a relatively small rise is followed by a downward trend not inconsistent with the anomalous decay at larger forces implied by the 4.2 μM fit in Fig. 1.

Author contributions: D.T. and M.E.F. designed research, performed research, contributed analytic tools, analyzed data, and wrote the paper.

The authors declare no conflict of interest.

*To whom correspondence should be addressed. E-mail: xpectnil@umd.edu.

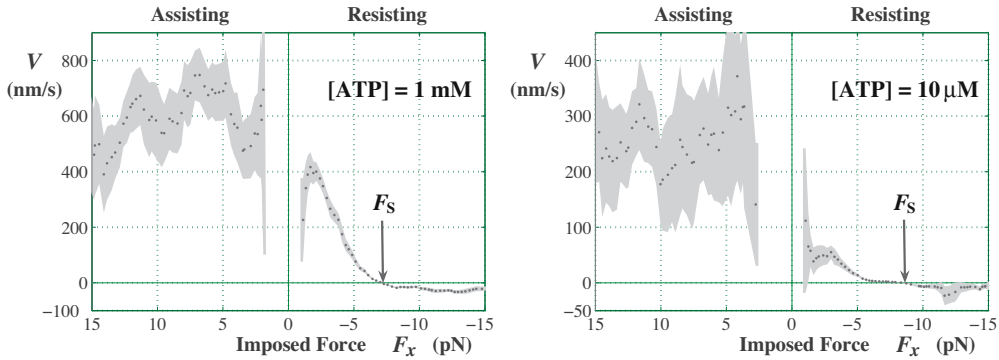

Fig. 2. Velocity vs. load for kinesin derived from observations of Carter and Cross (6). Detailed data for the fractions of forward and backward steps, π_+ and π_-, and corresponding dwell times, τ, as functions of a running (1.5 pN)-bin averaged force yield the velocity via $V = d(\pi_+ - \pi_-)/\tau$ (11, 12), where d = 8.2 nm represents the kinesin step size. The gray shading indicates the confidence intervals based on the number of observations.

Comparable velocity vs. load data for myosin V derived from observations by Mehta *et al.* (13) under resistive loading up to the stall force $F_S \simeq -2.8$ pN are shown in Fig. 3*a*. The original substall fits to these data (14) have been extrapolated analytically to both the assisting and large resisting ($F_x < F_S$) regimes (see Fig. 3*a*). For superstall loads, the fits closely merge, indicating an *independence* of [ATP]; then, in contrast to kinesin, the predicted velocity plunges rapidly to negative values exceeding 800 nm/s. For assisting loads, however, the implied behavior more closely reflects that for kinesin: the fits exhibit broad maxima that, ultimately, decrease to zero (although this is not evident graphically for high [ATP]).

Experiments by Gephardt *et al.* (15) ranging from $F_x = 10$ pN to -10 pN, serve to check these expectations. As evident from Fig. 3*b*, the extrapolated substall fits provide a remarkable (and even semiquantitative) description of the striking fall of $V(F_x)$ to large backward values. Note, especially, the observed independence of [ATP] beyond stall. Furthermore, the assisting-load measurements confirm the predicted saturation effect: for [ATP] = 1 μM, there is little increase above $V(0)$; while for 100 μM, even the anomalous decrease with increasing F_x seems confirmed.

In summary, in addition to seeking the origins of the large-load behavior of kinesin, one should ask why myosin V is so different in the superstall regime. More generally, how is it that simple two-state kinetic models, matching only data for low loads, extrapolate so successfully to both large assisting and resisting loads?

Free-Energy Landscape and Transition States

To make progress, consider the basic N-state kinetic model (4, 8, 9, 14) in which a mechanoenzyme in an initial or waiting state [0] binds a substrate molecule (e.g., ATP) and proceeds forward through a succession of N mechanochemical states ($j = 1, 2, \cdots$), completing a cycle by reaching the final state [N] that, biochemically, is identical to [0], while *mechanically* the enzyme has completed a forward "step": for a rotary motor (2, 3), this step could be an angular increment, $\Delta\theta$; but for a translocatory motor on a track (the situation on which we will focus), it will be a linear displacement, $d\,\hat{\mathbf{x}}$ [where $\hat{\mathbf{x}}$ is a unit vector and d is close to 8.2 nm for kinesin and 36 nm for myosin V (1, 2)]. Chemical reversibility demands that, for each forward transition from state (j) to (j+1) at a rate u_j, there is a reverse transition from (j+1) to (j) with a (nonvanishing) rate w_{j+1}.

To account for imposed loads one needs expressions for $u_i(\mathbf{F})$ and $w_i(\mathbf{F})$; these follow from a free-energy landscape picture (1, 4, 8, 9, 16, 17). The most primitive example, an ($N = 1$) model with just two rates, u_0 and w_0, is illustrated in Fig. 4. Here, the coordinate x locates the enzyme, a motor protein, as it moves on the periodic track. A free-energy barrier generates a transition state, marked by a cross, which must be overcome by thermal activation when the motor moves either forward or backward. As depicted, $\Phi(x)$ is periodic which implies no net forward drift: this corresponds to stall, that is, $V = 0$ and $\mathbf{F} = \mathbf{F}_S = (F_S, 0, 0)$.

However, on imposing a force $\mathbf{F}$ ($\neq\mathbf{F}_S$) the free-energy function becomes $\Phi(x) \Rightarrow \Phi(\mathbf{r}) - (\mathbf{F}-\mathbf{F}_S)\cdot\mathbf{r}$, where, for generality, we have identified a "point of attachment," P[$\mathbf{r} = (x, y, z)$], on the body of

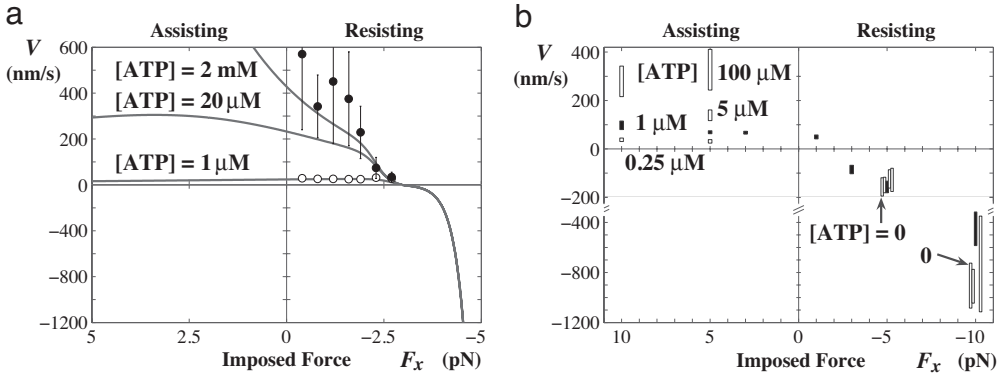

Fig. 3. Myosin V. (*a*) Substall data derived from Mehta *et al.* (13) fitted to a two-state kinetic model by Kolomeisky and Fisher (14) (evaluated here also for [ATP] = 20 μM). Note the factor of 2 scale change for negative, superstall velocities. (*b*) The velocity under superstall and large assisting loads [after Gebhardt *et al.* (15)]. The solid symbols represent data for [ATP] = 1 μM; those for $F_x = -$(5 and 10) pN have been narrowed and displaced slightly to distinguish data for [ATP] = 0, 0.25 μM up to 0.1 mM. Note the scale change for $V < -200$ nm/s.

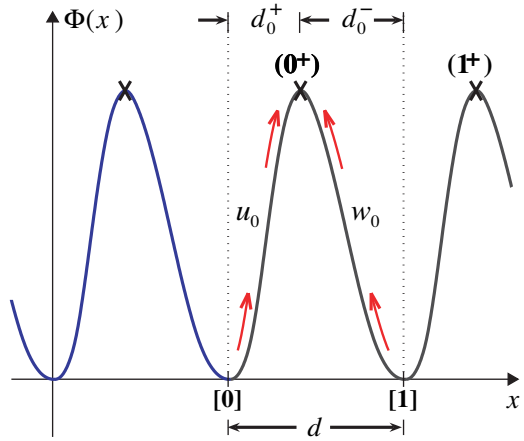

Fig. 4. The simplest one-dimensional free-energy landscape, $\Phi(x)$, where the coordinate x represents the point of attachment P on the motor at which the load force $\mathbf{F} = (F_x, 0, 0)$ is imposed. The transition states (0^+) and (1^+) are marked by crosses. Note that states [0] and [1] are biochemically equivalent although physically displaced; likewise, (0^+) and (1^+).

the motor. Thus, a substall force tilts the landscape potential downward lowering the barrier for a forward transition and, hence, increasing u_0 while the reverse transition rate, w_0, is reduced.

In general, as illustrated in Fig. 5, the landscape $\Phi(\mathbf{r})$ will be more complex and depend also on the z and y coordinates of P. Potential wells (or valleys) at locations $\mathbf{r}_j$ correspond to intermediate states (j). Reaction paths between neighboring states, (j) and $(j+1)$, traverse cols (or passes or saddles) that determine the associated *transition states* at $\mathbf{r}_j^+ = \mathbf{r}_{j+1}^-$ (see, e.g., ref. 9). To leading exponential order in $\mathbf{F}$, traditional reaction-rate theory then yields (1, 8, 9)

$$u_j(\mathbf{F}) = u_j^0 e^{\mathbf{F}\cdot\mathbf{d}_j^+/k_BT}, \quad w_j(\mathbf{F}) = w_j^0 e^{-\mathbf{F}\cdot\mathbf{d}_j^-/k_BT}, \qquad [1]$$

where the "partial substeps" are given by

$$\mathbf{d}_j^+ \equiv \boldsymbol{\theta}_j^+ d = \mathbf{r}_j^+ - \mathbf{r}_j \quad \text{and} \quad \mathbf{d}_j^- \equiv \boldsymbol{\theta}_j^- d = \mathbf{r}_j - \mathbf{r}_j^-, \qquad [2]$$

and obey $\Sigma_j(d_j^+ + d_j^-) = d$ (see, e.g., Fig. 4). The $\boldsymbol{\theta}_j^\pm$ are "load distribution vectors" or, neglecting the y and z components, "load distribution factors," $\theta_j^\pm$; they clearly sum to unity (4, 8, 9).

Velocities under Large Loads for $N = 1$

In the following we will appeal to formulas for V in terms of the set of $2N$ transition rates $\{u_j(\mathbf{F}), w_j(\mathbf{F})\}$ (see, e.g., ref. 18). To gain insight, however, let us initially neglect F_y and F_z and consider only the simplest case $N = 1$ for which $V/d = u_0(\mathbf{F}) - w_0(\mathbf{F})$. For the situation in Fig. 4 one may reasonably regard x as a reaction coordinate so that the transition state lies, physically, between states [0] and [1] and $0 < \theta_0^+ \equiv d_0^+/d < 1$. Then one finds (see curve b in Fig. 6) that *superstall* loads *necessarily* lead to large negative speeds, that is, *formally*, $V(F_x) \to -\infty$ as $F_x \to -\infty$, while *assisting* loads lead to the complementary behavior, that is, $V(F_x) \to +\infty$ as $F_x \to +\infty$. Thus, the expected or "normal" performance under large loads is mandatory in both regimes. Conversely, the unnatural or "anomalous" response seen in Figs. 1–3 (minima and decreasing reverse speeds at superstall and saturation/maxima for assisting force) *cannot* be captured!

It is crucial to realize, however, that the physical displacement x of the point of attachment, P, need *not* be an acceptable reaction coordinate. Indeed, the "minimal" adequate biophysiochemical or *enzymatic structural space* may entail the y and z coordinates of P and other "unseen" dimensions (8, 9, 16, 17). Thus, as illustrated in Fig. 7, the transition state may lie *outside* the natural domain $0 < x < d$. There are two new cases: first, if, as in Figs. 6*c* and 7, one has $\theta_0^+ = d_0^+/d > 1$, then, necessarily, **anomalous superstall behavior** is generated. See plot c in Fig. 6; formally, we can assert: $V(F_x) \to 0^-$ when $F_x \to -\infty$. Nevertheless, only normal behavior is realized under assisting loads: plots *b* and *c* in Fig. 6.

In the last case, $\theta_0^+ = d_0^+/d$ is *negative*, and superstall variation must be normal but **assisting-load anomalous behavior** arises, that is, $V(F_x) \to 0$ when $F_x \to +\infty$ (see Fig. 6*a*).

In all cases, the qualitative large-load behavior is *independent* of the specific values of the load-free rates, u_0^0 and w_0^0. In other words, the performance under superstall and assisting loads is determined only by *structural features* of the landscape $\Phi(x)$. Is that true more generally? If so, what are the crucial features? And when are *both* superstall and assisting-load behavior anomalous?

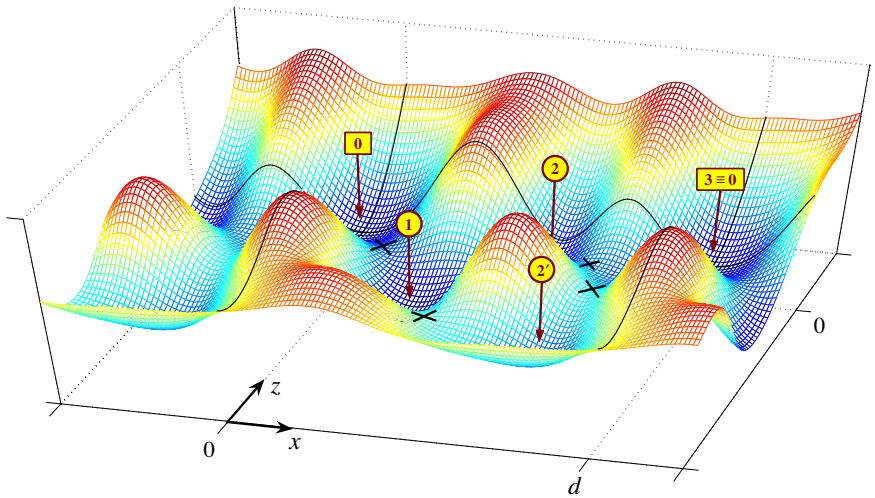

Fig. 5. An $(N = 3)$-state free-energy landscape, $\Phi(r)$, with locally stable intermediate states (j) for $j = 0, 1, 2, \cdots$, labeled and with an extra "side state" (2′). The neglect of the transverse y coordinate is justified if Φ increases rapidly with y^2. The transition states, at $\mathbf{r}_j^+ = \mathbf{r}_{j+1}^-$, are marked by crosses. If the pass between state (2′) and [3 ≡ 0] becomes sufficiently high, the (2′, 3) transitions will be suppressed: then a (1, 2′) transition represents a side reaction off the main reaction path [0] ⇌ (1) ⇌ (2) ⇌ [3] (see Figs. 8 and 9).

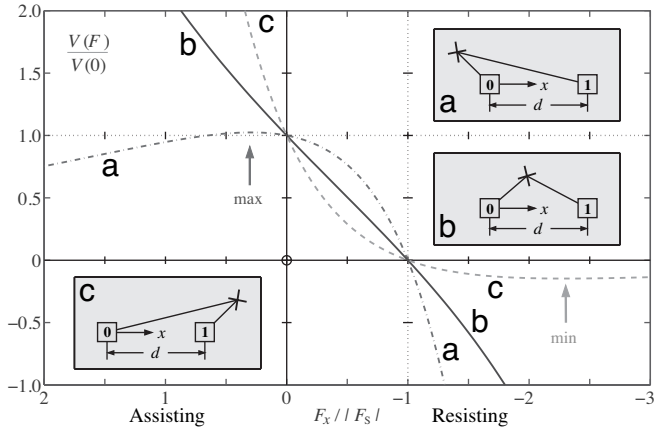

Fig. 6. Variation of velocity with imposed force for the ($N = 1$)-state model with, as specific examples, $u_0^0/w_0^0 = 4$ and load distribution factors: (*a*) $\theta_0^+ = -0.2$, (*b*) $\theta_0^+ = 0.4$, and (*c*) $\theta_0^+ = 1.2$; as depicted in *Insets a, b,* and *c*. Cases *b* and *c* correspond to Figs. 4 and 7. Recall, as in Fig. 4, that states [0] and [1] are biochemically equivalent.

N-State Sequential Motor Protein Models

Recall, now, that N-state sequential models are specified by 2N rates $\{u_i, w_j\}$ and $2N$ structural parameters, namely, $\{\mathbf{r}_j, \mathbf{r}_j^+\}$, the state and transition state locations of the attachment point, P. Fig. 8 portrays two complete cycles of an $N = 3$ system. Note that states (j) and $(j \pm N)$ and (j^+) and $(j^+ \pm N)$ are biochemically identical, although physically distinct; the corresponding periodicity conventions $\mathbf{r}_{j+kN} = \mathbf{r}_j + kd\,\hat{\mathbf{x}}$ and $\mathbf{r}_{j+kN}^{\pm} = \mathbf{r}_j^{\pm} + kd\,\hat{\mathbf{x}}$, for $k = \pm 1, \pm 2, \cdots$, are embodied in the figure.

To account for the vectorial nature of the force $\mathbf{F}$, we follow refs. 8 and 9, noting that the tether transmitting force to the motor body in a typical single-molecule bead assay (1, 4–7) is inclined, say at a polar angle Θ to the z axis. Hence, the experimentally controlled component F_x induces a *normal component* $F_z \propto |F_x|$ (8, 9). (We suppose $F_y \equiv 0$.) Although the orientation of the tether switches fairly abruptly (8, 9) when the load changes from resisting to assisting, the magnitude of Θ, mainly fixed by the bead diameter (8, 9), can be taken as constant. Consequently, in using Eq. **1** we may suppose

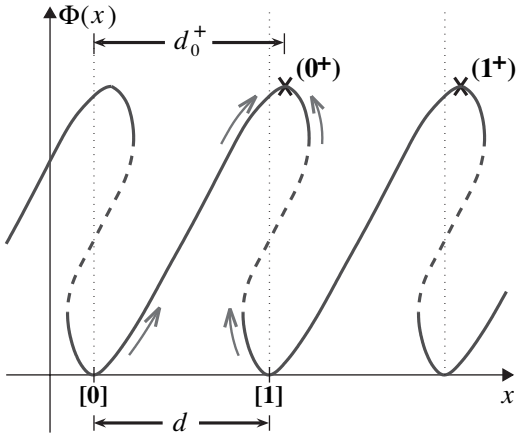

Fig. 7. A one-dimensional landscape, as in Fig. 4, but with a transition state displaced so that $\theta_0^+ = d_0^+/d > 1$. Various portions of the plot should be regarded as projected from other physical or chemical dimensions (so that the free-energy Φ remains single-valued as a function of an appropriate reaction coordinate).

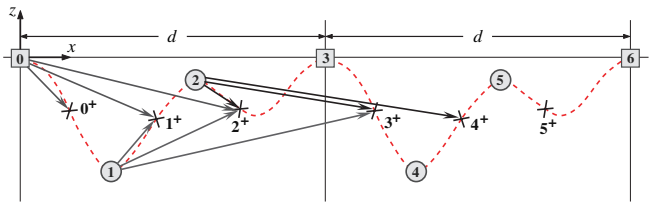

Fig. 8. Two cycles of an ($N = 3$)-state sequential model corresponding to Fig. 5 projected on to the (x, z) plane but neglecting state (2′). The locations of states (j) and transition states (j^+) are displayed along with $N^2 = 9$ significant structural vectors, $\mathbf{r}_{i+j}^{\pm} - \mathbf{r}_i$, for $i = 0, 1, 2$, that is, $(\mathbf{r}_0^+ - \mathbf{r}_0)$, $(\mathbf{r}_1^+ - \mathbf{r}_0)$, $(\mathbf{r}_2^+ - \mathbf{r}_0)$, $(\mathbf{r}_1^+ - \mathbf{r}_1)$, etc. Recall that states [0], [3], and [6] are biochemically equivalent, as are states (1) and (4), (2) and (5), etc.

$$\mathbf{F} = F_x\mathbf{c}^{\pm} \quad \text{for} \quad F_x \gtrless 0 \quad \text{with} \quad \mathbf{c}^{\pm} = (1,\ 0,\ \pm c_{\parallel}), \qquad [3]$$

where $c_{\parallel} = \cot\Theta > 0$. [For kinesin one has $c_{\parallel} \simeq 1.45$ (9).]

Now, by employing known theory (18), one may write the turnover rate, or reduced velocity, in the form (12)

$$\frac{V}{d} = \frac{1 - \exp[-(F_x - F_S)d/k_BT]}{\sum_{i=0}^{N-1}\sum_{j=0}^{N-1} K_{i,j}\exp[-F_xD_{i,j}^{\pm}/k_BT]}, \qquad [4]$$

where the N^2 force-independent inverse rate parameters $K_{i,j}$ are nonvanishing, positive ratios of various products of the zero-load rate constants $\{u_k^0, w_l^0\}$. However, the force dependence for $F_x \gtrless 0$ is controlled by the $2N^2$ key geometrical parameters

$$D_{i,j}^{\pm} = \mathbf{c}^{\pm}\cdot(\mathbf{r}_{i+j}^{+} - \mathbf{r}_i) = x_{i+j}^{+} - x_i \pm c_{\parallel}(z_{i+j}^{+} - z_i), \qquad [5]$$

for $i, j = 0, 1, \cdots, N-1$. These may be regarded as projections on to $\mathbf{c}^+$ and $\mathbf{c}^-$ (for $F_x \gtrless 0$) of the vectorial substeps from a state $\mathbf{r}_i$ to the transition state $\mathbf{r}_{i+j}^{+}$. See, for example, the nine vectors from states [0], (1), and (2) in Fig. 8 given by $j = 0$, 1, and 2.

Now the way is clear! When large superstall loads are tested (formally, $F_x \to -\infty$), Eq. **4** yields $|V| \approx \exp[|F_x|(d - D_{\max}^{-})/k_BT]$, where $D_{\max}^{-}$ is the largest projection $D_{i,j}^{-}$. Consequently, we can conclude, in words:

A: Anomalous superstall variation, $V \to 0^-$, results if but only if *at least one* of the N^2 projections $D_{i,j}^{-}$ *exceeds* the step size d.

Note that this justifies the conclusion illustrated in Fig. 6*c*. Inspection of Fig. 8, however, reveals that the landscape of Fig. 5 [without state (2′)] *cannot* yield anomalous superstall behavior but *could* do so if the coordinate x_1 became smaller than x_0^+.

The complementary argument for $F_x > 0$ applied to Eq. **4** (formally, $F_x \to +\infty$) clearly yields:

B: Assisting-load anomalous behavior, V decreasing, is realized if but only if *at least one* of the N^2 projections $D_{i,j}^{+}$ is *negative*.

This bears out the convex form of Fig. 6*a* but shows that only normal assisting load performance is realizable for the system in Fig. 8. Furthermore, when $N = 1$ there is only one term in the denominator in Eq. **4**; thus, an anomalous response for both signs of F_x is forbidden unless $N \geqslant 2$. Conversely, as demonstrated by Fig. 1 (8), two-state models can be *doubly anomalous*.

Colocalization and Fuel Dependence

The structural projections in Eq. **5** are expressible by using the load distribution vectors, $\boldsymbol{\theta}_i^{+}$ and $\boldsymbol{\theta}_j^{-}$ (see Eq. **2**). Thus, in Fig. 8, one has $D_{j,0}^{+} = \mathbf{c}^{+}\cdot\boldsymbol{\theta}_j^{+}d$, $D_{j,1}^{+} = \mathbf{c}^{+}\cdot(\boldsymbol{\theta}_j^{+} + \boldsymbol{\theta}_{j+1}^{-} + \boldsymbol{\theta}_{j+1}^{+})d$, etc., and, using the periodicity, for example,

$$D_{j,N-1}^{-} = \mathbf{c}^{-}\cdot(\mathbf{r}_{j+N}^{-} - \mathbf{r}_j) = d(1 - \mathbf{c}^{-}\cdot\boldsymbol{\theta}_j^{-}), \qquad [6]$$

and so on. Now it may happen that to a good approximation a transition state, say (j^+) or (j^-), and an adjacent biochemically distinct state, say (j), are *physically colocalized* so that $\boldsymbol{\theta}_j^{+} =$

$(\mathbf{r}_j^+ - \mathbf{r}_j)/d$ or $\boldsymbol{\theta}_j^- = (\mathbf{r}_j - \mathbf{r}_j^-)/d$ vanishes. Thus, real biochemical changes, $(j-1) \rightleftharpoons (j^-) \rightleftharpoons (j) \rightleftharpoons (j^+) \rightleftharpoons (j+1)$, occur, but the point of attachment, P(x, y, z), on the motor undergoes no appreciable displacement in the step $(j) \rightleftharpoons (j^+)$ or in the step $(j^-) \rightleftharpoons (j)$ [although, of course, (j^+) or (j^-) will likely differ from (j) in significant but unseen dimensions]. The corresponding vanishing of $D_{j,0}^+$ then implies, by Eq. **4** and **B**, that *under large assisting loads* $V(F_x)$ will saturate, that is, approach a *maximal value.*

Similarly, under resisting forces, the associated equality $D_{j,N-1}^- = d$ that follows from Eq. **6**, takes one to the borderline at which *anomalous superstall behavior* sets in (see **A**). Accordingly, the backward velocity is then expected to *decelerate* as $|F_x|$ increases above F_S and approach a limiting or minimal negative value.

In application of kinetic models to motor proteins, the supply of molecular fuel or substrate, say ATP, is well represented by taking $u_0^0 = k_0^0$[ATP] as the initial, zero-load rate; the stall force can then be set by a corresponding form for the reverse rate w_0^0 (or w_{N-1}^0, etc.) (see refs. 4, 8, 14, and 19). The dependence or otherwise of the large-load velocity on the fuel supply, as noted in connection with myosin V in Fig. 3, hinges, therefore, on the inverse rate parameters $K_{i,j}$ in Eq. **4**. When $|F_x| \to \infty$, one of the N^2 terms in the denominator will dominate exponentially and carry a corresponding inverse rate, say K^- or K^+ for $F_x \gtrless 0$. If these particular parameters do not depend on [ATP], that is, do not carry u_0^0 as a factor [or, possibly, w_0^0, etc. (14, 19)], the large load response will be independent of [ATP], and vice versa. For a given landscape this can be checked from expressions for $K_{i,j}$ (12).

Side-Reaction Paths

Experiments on RNA polymerase (20) have observed "pauses" in otherwise steady stepping along the DNA track. Such intermittent motions suggest the presence of reaction side chains that branch off the main pathway (see Fig. 9). The previous theory is readily generalized for side-reaction chains (and trees, etc.) (12, 18). If a sequence of L states, located, say, at $\mathbf{r}_k^s$ for $k = 1, 2, \cdots, L$, springs from state (s) at $\mathbf{r}_s \equiv \mathbf{r}_0^s$, one needs $2NL$ further structural parameters to extend conclusions **A** and **B**: these are the vector projections

$$D_{j,k}^{s\pm} = \mathbf{c}^{\pm} \cdot (\mathbf{r}_{s+j}^{+} - \mathbf{r}_k^s), \quad j = 0, 1, \cdots, N-1, \qquad [7]$$

and each is associated with an inverse rate parameter $K_{j,k}^s$ as in Eq. **4**, but entailing also the side-reaction zero-load transition rates $\{u_{k-1}^0, w_k^0\}$ (12). For the example in Fig. 9 the corresponding $LN = 1 \times 3$ new vectors have been drawn in.

Both anomaly assertions **A** and **B** now remain valid provided that one supplements "the N^2 projections $D_{i,j}^{\pm}$" (or "$D_{i,j}^{+}$," respectively) by "and the LN projections $D_{j,k}^{s-}$" (or "$D_{j,k}^{s+}$"). Application to the side-reaction system of Fig. 9, where the vector $(\mathbf{r}_1^+ - \mathbf{r}_{2'})$ has a relatively large negative x component, reveals a surprise: whenever $c_\parallel$ is not too large, the assisting-load (V, F_x) profile will be *anomalous* (even though a normal superstall response remains).

If there are a number of side paths, one need only include the extra vector projections in the anomaly condition list (12).

Parallel Pathway Mechanoenzymes. Various lines of evidence (4) suggest a need for models with alternative pathways to achieve cycle completion. In the simplest case, two independent parallel pathways of N_α and N_β transitions run from the unique state [0] via (1_α) or (1_β) to $(N_\alpha - 1)$ or $(N_\beta - 1)$ and meet again at $[N_\alpha] \equiv [N_\beta]$. Kolomeisky (21) has obtained exact results for V that can be recast (and extended to multiple parallel pathways) as a sum of two terms, $V_\alpha + V_\beta$, each with (by appeal to detailed balance) the *same* numerator as in Eq. **4**. The denominators are distinct

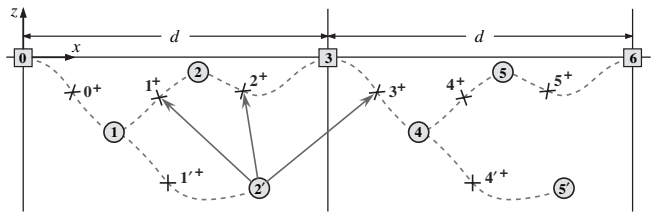

Fig. 9. Two cycles of the three-state model in Fig. 8 augmented by a side-reaction path of length $L = 1$ branching from state (1) to state (2′) yielding three additional significant structural vectors.

but coupled together (12). Then $2(N_\alpha^2 + N_\beta^2)$ structural parameters, $D_{i,j}^{\alpha\pm}$ and $D_{l,m}^{\beta\pm}$, can be defined in *precise* analogy to Eq. **5**; these suffice to determine the large-load behavior.

Because the two chains are linked at state [0], it proves essential to distinguish the corresponding projections, $D_{0,j}^{\alpha\pm}$ and $D_{0,m}^{\beta\pm}$, from those with roots at $i, l \neq 0$. Then we may introduce $N_{\alpha\beta} \equiv N_\alpha N_\beta (N_\beta - 1)$ "coupled projections" by

$$D_{j;l,m}^{\alpha\beta-} = D_{0,j}^{\alpha-} + D_{l,m}^{\beta-} - \max_n D_{0,n}^{\beta-}, \qquad [8]$$

where $j, m \geqslant 0$ while $l \geqslant 1$. The $N_{\beta\alpha} \equiv N_\beta N_\alpha (N_\alpha - 1)$ parameters $D_{m;i,j}^{\beta\alpha-}$ are defined similarly (with $i \geqslant 1$), while for the complementary $N_{\alpha\beta}$-coupled projections, $D_{j;l,m}^{\alpha\beta+}$ and $D_{m;i,j}^{\beta\alpha+}$, min replaces max. Finally, the first anomaly condition can be stated as:

A$^\parallel$ Anomalous superstall variation is realized if but only if, first, *at least one* of the $(N_\alpha^2 + N_{\alpha\beta})$ α-projections, $D_{i,j}^{\alpha-}$ and $D_{j;l,m}^{\alpha\beta-}$, *and*, second, *at least one* of the $(N_\beta^2 + N_{\beta\alpha})$ β-projections, $D_{l,m}^{\beta-}$ and $D_{m;i,j}^{\beta\alpha-}$, exceeds the step size d.

The complementary condition **B$^\parallel$** for **assisting load anomalies** follows merely by replacing each superscript minus sign in **A$^\parallel$** with a plus sign and changing the final phrase to "is negative."

These parallel pathway criteria for anomalous behavior seem more demanding than for two distinct single chains. Nevertheless, the coupling actually provides extra possibilities beyond the single-chain requirements. To see this, suppose $N_\alpha = N_\beta = 2$ and, for simplicity, consider $c_\parallel = 0$ so that only the *scalar* load distribution sets, $\Theta_\alpha \equiv (\theta_{\alpha 0}^+, \theta_{\alpha 1}^-, \theta_{\alpha 1}^+, \theta_{\alpha 0}^-)$ and Θ_β, are needed to specify the α- and β-chain structures. The concrete assignments

$$\Theta_\alpha = \tfrac{1}{10}(5, 1, 2, 2) \quad \text{and} \quad \Theta_\beta = \tfrac{1}{10}(5, -1, 3, 3), \qquad [9]$$

which verify $\Sigma_j \theta_{\lambda j}^{\pm} = 1$, then prove instructive.

By way of Eq. **5**, these yield the sets $\{D_{i,j}^{\alpha\pm}\}$ and $\{D_{l,m}^{\beta\pm}\}$ of $N_\alpha^2 + N_\beta^2 = 4$ basic structural projections for each chain, namely,

$$(0.5, 0.8; 0.2, 0.9)d, \quad \text{and} \quad (0.5, 0.7; 0.3, 1.1)d, \qquad [10]$$

where $i, j, l, m = 0, 1$. Consider first each chain individually: from the criteria **A** and **B** one sees that the α-chain cannot display anomalous (V, F_x) profiles. Since $D_{11}^{\beta\pm} > d$, however, the β-chain will be anomalous above stall: this is a consequence of the negative load factor $\theta_{\beta 1}^-$, as is easily seen in a plot like Fig. 8.

But when the two chains are coupled we must appeal to **A$^\parallel$** and use Eq. **1** to compute the $N_{\alpha\beta} = 4$ *coupled projections*, noting first from Eq. **10**, that $\max_n(D_{0,n}^{\beta-}) = 0.7d$ whence one finds

$$\{D_{j;l,m}^{\alpha\beta}\} = (0.1, 0.9; 0.4, 1.2)d \quad \text{for} \quad l = 1, \quad j, m = 0, 1. \qquad [11]$$

Since $D_{1;1,1}^{\alpha\beta}$ exceeds d we conclude that the coupled (α,β) chains will, in fact, jointly exhibit anomalous superstall behavior. Lastly, it should be remarked that side reactions branching off one or both pathways can be handled analytically just as explained above for the sequential models (12). Explicit analytical results

have also been found (12) for *looped side reactions* in which a transition sequence of $M \geq 2$ steps branches off from a particular state to which it returns on the last step. However, the possible role of such "isolated futile cycles" is not presently clear.

Discussion

Our analysis of the conditions under which large loads lead to anomalous (V, F_x) responses might well be explored for other enzyme schemes. Most pressing perhaps are *divided pathway systems*, in which, after N_γ (>1) steps, the enzyme can proceed by two distinct routes, say α and β, that meet again with N_δ (≥ 0) steps remaining before the full cycle is completed. Fig. 5 represents a (1, 2, 2, 0) example. There is, indeed, evidence that myosin V has such a significant alternative pathway (22, 23). A closed formulation for $V(F_x)$ in terms of all of the $2\Sigma_\lambda N_\lambda$ rates has been derived (12). On using that, explicit criteria emerge regarding the large-load behavior, but they lack the intuitive clarity and relative simplicity exemplified in the anomaly rules **A**, **B**, $\mathbf{A}^{\|}$, and $\mathbf{B}^{\|}$ derived above. Specifically, *disconnected four-state* vector differences, such as $(\mathbf{r}_i^+ - \mathbf{r}_j + \mathbf{r}_k^+ - \mathbf{r}_l)$, appear and must also be used.

Rather than describe a systematic algorithm for still more complex kinetic models (12) let us reflect briefly on the results obtained. Foremost is the fact that mechanoenzyme performance under large imposed forces is determined by a relatively few general parameters that physically locate specific *transition states* relative to intermediate biomechanochemical states.

Furthermore, as already demonstrated for kinesin (8), allowance for motions of the enzyme normal to the track, or, generally, in the full (x, y, z) space, may be crucially important. Likewise significant is the recognition, illustrated in Figs. 6 and 7, that a mechanochemical transition state *need not* lie "physically" between the biophysical states it links. This recognizes that the obvious physical coordinate measuring the progress of a mechanoenzyme may not be a satisfactory reaction coordinate: thus, as in Figs. 6 and 7, "local backtracking" may occur even though the enzymatic transitions move steadily forward (11).

Recall next, the observations in Figs. 1–3 demonstrating that reverse motions and their fuel dependence under superstall loads can be successfully predicted by simple kinetic models and smoothly linked to substall performance without invoking further mechanisms. These facts bring into question various proposals (e.g., refs. 10 and 15), arguing that new effects and special phenomena should enter when, under the imposition of a large resistive load, a mechanoenzyme progresses backward. Although novel features could play a role when a mechanoenzyme is reversed by overload, one might, in the absence of contrary evidence, rather hold that the fundamental biophysiochemical picture of a series of reactions being reversed merely by tilting the free-energy landscape, that is, altering the balance of free energy, should be accepted as the primary hypothesis.

Finally, when an imposed force is switched from resisting or opposing, as usually considered normal for mechanoenzymes, to assisting or helping, it is certainly reasonable to allow for specific mechanical changes; merely reversing the sign of F_x in a formula fitted for $F_x < 0$ is unlikely to prove adequate. In our analysis this was recognized explicitly by introducing in Eq. **3** the projection vectors $\mathbf{c}^{\pm}$ that allow for the tether orientation. But, in a detailed analysis of kinesin (8), a further specific mechanism was invoked on the basis of the experimental data (7). Nevertheless, the paramount role of the geometrical location of states and transition states should remain under large assisting forces just as in the superstall regime.

We thank Dr. Martin Lindén and Professor A. B. Kolomeisky for their interactions and correspondence and Professor D. Thirumalai for his ongoing interest. Professor R. A. Cross kindly made his kinesin data available to us, and he, Professor E. W. Taylor, and N. R. Guydosh commented on a draft.

1. Howard J (2001) *Mechanics of Motor Proteins and the Cytoskeleton* (Sinauer, Sunderland, MA).
2. Schliwa M, ed (2003) *Molecular Motors* (Wiley–VCH, Weinheim).
3. Berg HC (2003) *Annu Rev Biochem* 72:19–54.
4. Kolomeisky AB, Fisher ME (2007) *Annu Rev Phys Chem* 58:675–695, and references therein.
5. Block SM, Asbury CL, Shaevitz JW, Lang MJ (2003) *Proc Natl Acad Sci USA* 100:2351–2356.
6. Carter NJ, Cross RA (2005) *Nature* 435:308–312.
7. Lang MJ, Asbury CL, Shaevitz JW, Block SM (2002) *Biophys J* 83: 491–501.
8. Fisher ME, Kim YC (2005) *Proc Natl Acad Sci USA* 102:16209–16214.
9. Kim YC, Fisher ME (2005) *J Phys Condens Matter* 17:S3821–S3838.
10. Molloy JE, Schmitz S (2005) *Nature* 435:286–287.
11. Tsygankov D, Lindén M, Fisher ME (2007) *Phys Rev E* 75(021909):1–16.
12. Tsygankov D, Fisher ME (2007) *J Chem Phys*, 127.
13. Mehta AD, Rock RS, Rief M, Spudich JA, Mooseker MS, Cheney E (1999) *Nature* 400:590–593.
14. Kolomeisky AB, Fisher ME (2003) *Biophys J* 84:1642–1650.
15. Gebhardt JCM, Clemen AE-M, Jaud J, Rief M (2006) *Proc Natl Acad Sci USA* 103:8680–8685.
16. Keller D, Bustamante C (2000) *Biophys J* 78:541–556.
17. Xing J, Wang H, Oster G (2005) *Biophys J* 89:1551–1563.
18. Kolomeisky AB, Fisher ME (2000) *Physica A* 279:1–20, erratum (2000) 284:496.
19. Fisher ME, Kolomeisky AB (2001) *Proc Natl Acad Sci USA* 98:7748–7753.
20. Wang MD, Schnitzer MJ, Yin H, Landick R, Gelles J, Block SM (1998) *Science* 282:902–907.
21. Kolomeisky AB (2001) *J Chem Phys* 115:7253–7259.
22. Uemura S, Higuchi H, Olivares AO, De La Cruz EM, Ishiwata S (2004) *Nat Struct Mol Biol* 11:877–883.
23. Baker JE, Krementsova EB, Kennedy GG, Armstrong A, Trybus KM, Warshaw DM (2004) *Proc Natl Acad Sci USA* 101:5542–5546.